

Seismic Broadband Ocean-Bottom Data and Noise Observed with Free-Fall Stations: Experiences from Long-Term Deployments in the North Atlantic and the Tyrrhenian Sea

by T. Dahm, F. Tilmann, and J. P. Morgan

Abstract In a comparative study of two long-term deployments we characterize the seismic noise on the seafloor in the North Atlantic south of Iceland and in the Tyrrhenian Sea north of Sicily. We estimate the teleseismic body-wave detection threshold to be approximately magnitude 6.0 at frequencies below the microseismic band ($f < 0.1$ Hz) on vertical components at the quietest sites in both regions. At the microseismic peak (~ 0.25 Hz) in the North Atlantic, the minimum magnitudes for events to be recorded most of the time are M_w 7.0 for the Tyrrhenian Sea deployment and above 8 for the North Atlantic deployment. By correlating seismic noise and oceanic waveheight amplitudes we are able to find the major generation areas of microseismic noise in the North Atlantic. Although the high noise of secondary microseisms at 0.24 Hz is generated far away from the ocean-bottom stations at three near-coastal regions, the microseismic noise at about 1 Hz is generated directly at the stations. We present a technique to estimate the noise generation areas prior to future deployment by using noise at nearby land stations.

The ambient low-frequency noise below 0.1 Hz occurs mainly on horizontal components and is probably induced by seafloor-current-induced tilt. The power spectral density of this noise varies by a factor of up to 10,000 between different stations and deployment sites, indicating in some cases wobbling deployments, possible problems of frame weakness, and a possible higher noise sensitivity of external packs to seafloor currents. Cross-coupling between horizontal and vertical channel noise is strong at some of our stations, demonstrating that the leveling mechanics can be further improved to reduce vertical channel noise.

Introduction

The number of temporary deployments of broadband seismological arrays on the ocean bottom will rapidly increase in the near future, because the technology is now available and the key processes of plate formation at mid-ocean ridges and plate destruction at subduction zones occur wholly or partly underneath the oceans. For example, Ritsema and Allen (2003) point out that large-aperture, passive ocean-bottom seismometer (OBS) experiments are necessary to give conclusive evidence for or against the existence of whole-mantle plumes, currently a point of strong controversy. Array apertures of at least 1000 km are needed to resolve structures below 400 km depth. Using a seismological array with an aperture of 300–500 km only, for example, a land-based array on Iceland, it is difficult to discriminate plumes from small-scale upper mantle convection or normal thermal fluctuations. In general, islands associated with other oceanic hotspots are even smaller than Iceland, for example, resulting in even lower resolvable maximum depths there.

Despite the obvious need for long-term seafloor deployments these experiments have so far only rarely been carried out. There are many reasons: first, a large technical and logistical effort is necessary to collect ocean-bottom broadband data. Second, a large number of suitable ocean-bottom stations did not exist until recently and they are still not available for the majority of seismologists. Third, the seismic noise on the seafloor is often much larger than on land. The body waves from a magnitude 7 earthquake recorded at about 70° epicentral distance may easily be hidden in the noise of a seafloor station, whereas an M_w 7 earthquake usually generates beautiful seismograms on a permanent land station at the same distance (Webb, 1998).

The general sources of seafloor noise are well understood. Since the early days of quantitative seismology a hundred years ago it has been suggested that oceanic gravity waves generate strong noise signals on the seafloor but also at inland stations hundreds of kilometers from the coastlines.

The primary microseismic peak at 0.1 Hz is not always visible and is assumed to be related to the interaction of oceanic waves and the coastlines, but the details of this interaction are not well understood. We only observe the secondary microseismic peak at 0.2–0.4 Hz; it is thought to be generated by a nonlinear frequency-doubling effect, which occurs when oceanic swell waves cross and standing waves develop (e.g., Longuet-Higgins, 1950; Hasselmann, 1963; Webb, 1998; Bromirski, 2001; Essen *et al.*, 2003). Microseismic noise at higher frequencies is thought to be related to cross-wind-driven waves (e.g., Webb, 1998).

It is of great interest to know the noise conditions of a region prior to planning an expensive ocean-bottom experiment. For example, the experiment has to be planned for a sufficiently long deployment period to obtain the required event coverage. Alternatively, suitable targets or deployment periods with low expected noise levels might be selected according to predicted noise levels. In certain cases, a better knowledge of noise sources and generation mechanisms might allow enhancement of the signal-to-noise ratio by processing, or guide the development of new deployment strategies, for example, by burying the sensor (e.g., Collins *et al.*, 2001).

In the following, we give examples of broadband OBS recordings of teleseismic earthquakes measured at different sites during two different deployments. The data were acquired with free-fall OBS from GEOMAR (Kiel) and the University of Hamburg. A systematic comparison of noise measurements reveals problems with the station design of some of our OBSs and helps to quantify detection thresholds for body and surface waves. Some of the deployed stations recorded strong noise at frequencies below 0.1 Hz, which could be attributed to tilt-induced noise. This noise could, in parts be removed from the vertical component by using the horizontal components (see following). In an extreme case, the sensor was apparently tilted from the horizontal by about 7°; the largest apparent tilt value reported by the analysis was 34°, but this value is likely to reflect problems with the instrument rather than actual tilt. By using the correlation between seismic and ocean-wave data we confirm that microseismic noise at frequencies near 1 Hz is generated by oceanic wave action near the station, whereas lower-frequency microseismic noise (~0.25 Hz) is correlated to wave action in a few relatively narrow generation areas in the North Atlantic, that is, off-shore the northwest coasts of Scotland and Ireland, on the Reykjanes Ridge south of Iceland, and in a band between North Iceland and West Norway. The generation areas are dominant presumably because the submarine topography and the preferential wind-wave directions are particularly favorable toward conversion of oceanic wave energy into secondary microseismic energy.

Recordings of Teleseismic Earthquakes and Tilt-Induced Noise

Between April and July 2002, GEOMAR and the Institute of Geophysics, University of Hamburg, installed a pas-

sive seismological network in the North Atlantic south of Iceland for three and a half months. Ten free-fall stations were deployed, of which nine have been successfully recovered. Four were Hamburg-type wideband stations (three-component PMD-113 seismic sensor from PMD Scientific, Inc., and a piezoelectric hydrophone, ob20, ob21, ob26, ob28); the others were GEOMAR-type stations, of which there were three four-component stations (PMD seismometer and differential pressure gauge, DPG [Cox *et al.*, 1984] [ob24], PMD seismometer and hydrophone [ob29], Lamont-Doherty Earth Observatory [LDEO] seismometer [Webb *et al.*, 2001] and DPG [ob23]) and three were one-component stations equipped with a DPG (ob25) or hydrophone (ob22, ob27) only. Station design and configuration are described in more detail in Dahm *et al.* (2002) and Flueh and Bialas (1999). The LDEO sensor has a flat acceleration response and thus lower output at low frequencies than the PMD sensor, which has a flat velocity response up to 0.02 Hz.

The station depth varied between 540 m at the youngest sample point beneath the Reykjanes Ridge (ob24) to 2780 m depth at the oldest point of the European plate (ob21). The network was designed as a large aperture array of about 500 km width and with a station–station distance of about 150 km or more (Fig. 1) to serve as a pilot study for a possible future large tomographic study beneath the Iceland hotspot. Body waves from earthquakes in the Aleutian, Kamchatka, or Japan regions sample the depth range of about 500 km beneath the Iceland hotspot before being recorded at one of the OBS stations.

Figure 2 shows the instrument-deconvolved and band-pass-filtered waveforms for a M 7.3 teleseismic earthquake in Kamchatka at a depth of 566 km and epicentral distances of 72–74°. Seven stations were operational and recorded the body and surface waves. Station ob21 has a fairly good signal-to-noise ratio (SNR) on both hydrophone and seismometer and recorded a seismogram comparable to the seismogram from the broadband land station in Reykjavik (BORG). The vertical channels of the other Hamburg-type stations (ob26, ob28) are noisier below 0.1 Hz. A large portion of this low-frequency noise was tilt induced and could be corrected for, as discussed subsequently (the figure shows traces after tilt correction). The noise level on the hydrophones varies strongly from station to station; this variability is unusual but must be related to local effects because identical hydrophones were used at each site.

Of the GEOMAR stations, only ob23 recorded four channels for this event; the vertical channel has a SNR comparable to that of the Hamburg-type stations in this example. The DPG records (ob23, ob25) show large low-frequency noise apparently related to infragravity waves; the frequency of these waves ($< \sim 0.025$ Hz for the station depths at 743 and 802 m at ob23 and ob25, respectively) is below the corner frequency of the DPG sensor, but the roll off of sensitivity is gentle enough for those waves to dominate the raw DPG noise spectrum nonetheless. The GEOMAR hydrophones (ob22, ob27) only show noise in Figure 2 but they

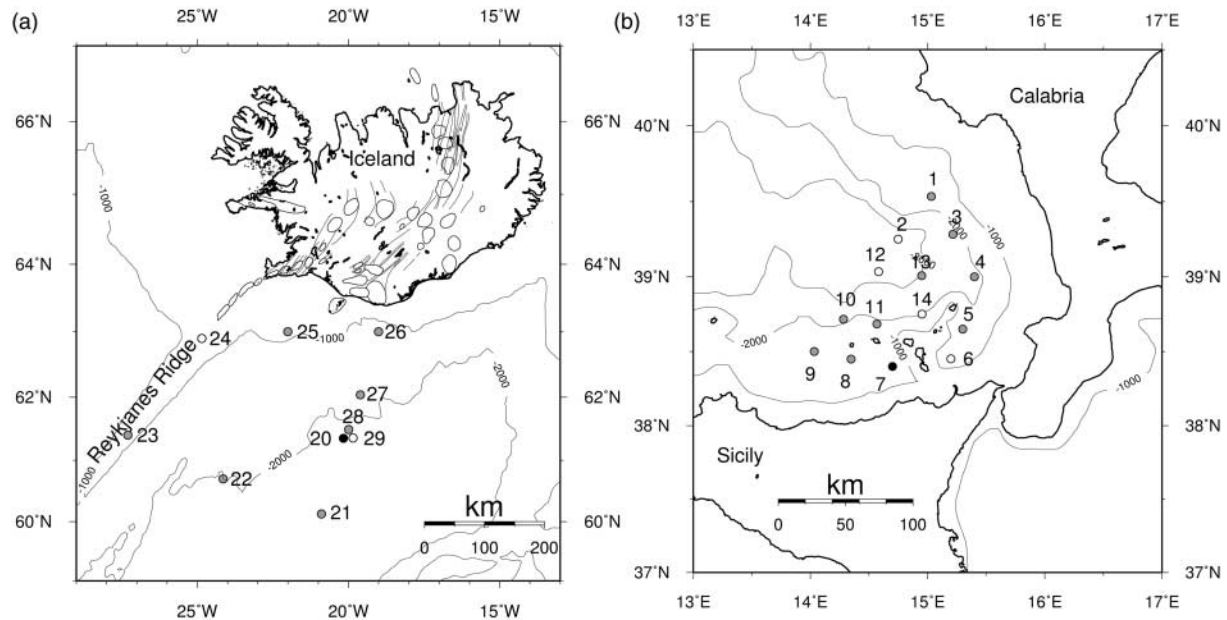


Figure 1. OBS stations deployed in the North Atlantic between April and July 2002 (a) and in the Tyrrhenian Sea between December 2000 and May 2001 (b). The open circles indicate stations that had technical problems with sensors or power consumption and therefore partially operated for only a few days. The stations marked by the filled circles were not recovered for unknown technical reasons. Stations 7, 8, 10, 11, 20, 21, 26, and 28 were Hamburg type, the others were GEOMAR type. The isolines indicate water depth in meters. Volcanic centers and fissure zones in Iceland are indicated by lines. See text for further explanations.

recorded earthquake signals at higher frequencies, above the upper corner of the filter (0.1 Hz) used in the preparation of Figure 2.

From December 2000 to May 2001 the same types of stations were deployed in a pilot study in the Tyrrhenian Sea (e.g., Dahm *et al.*, 2002). The array consisted of 14 stations with an aperture of about 150 km and interstation distances of about 25 km. Instruments included three Hamburg-type OBS stations (ob08, ob10, ob11), two GEOMAR-type OBS stations (ob05, ob06), and nine pure OBH (hydrophone or DPG only) stations from GEOMAR. The oceanic waveheight, and thus the microseismic noise peak, is much smaller in the Tyrrhenian Sea than in the North Atlantic. As expected, the waveforms collected during this pilot study have a better SNR and the detection threshold for teleseismic body waves is much lower than in the North Atlantic.

Figure 3 shows a waveform example for a M 6.7 shallow earthquake at 84° epicentral distance. GEOMAR-type station ob05 was equipped with a LDEO sensor, and Hamburg-type stations ob10 and ob11 were equipped with PMD sensors. At least on ob10 and ob11, even horizontal channels recorded acceptable seismograms, which are suitable for analysis of SKS shear-wave splitting (Rümpker, personal comm., 2004) and receiver functions (see Thorwart and Dahm, 2005).

It is well known that a bad leveling of seismic sensors generates cross-coupling between horizontal and vertical

channels. On the seafloor, the noise on the horizontal channels below 0.1 Hz is often a factor of 10 or more higher than on the vertical. The amplitude of this noise varies primarily on a timescale of days, but also shows a small dependence on semidiurnal tides. It is probably related to transient rotations of the stations induced by seafloor currents. Such tilt noise appears to first order only on the horizontal components. However, for a poorly leveled sensor the horizontal noise is transferred to the vertical component, resulting in a high coherence between noise measured on the vertical and horizontal channels. Crawford and Webb (2000) and Stutzmann *et al.* (2001) have demonstrated that the tilt noise on the vertical channel can be reduced by subtracting the cross-over signal predicted from the horizontal recordings. Their technique works well when horizontal components are recording mainly current-induced noise (tilt noise). As a by-product it provides an estimate of the actual tilt angle of the sensor on the seafloor. In Appendix A we briefly describe their technique as implemented here.

Inspection of the recordings at ob28 for a magnitude 6.5 earthquake show the strong improvement effected by the tilt correction (Fig. 4a,b). No arrivals are visible on the uncorrected record, but P , PP , S , SS , further phases, and surface waves are clearly visible on the corrected trace. At ob28, power spectral density (PSD) SNRs averaged over several earthquakes are improved by factors of 10 to 100 for the vertical channel, but they still fall short of the signal quality

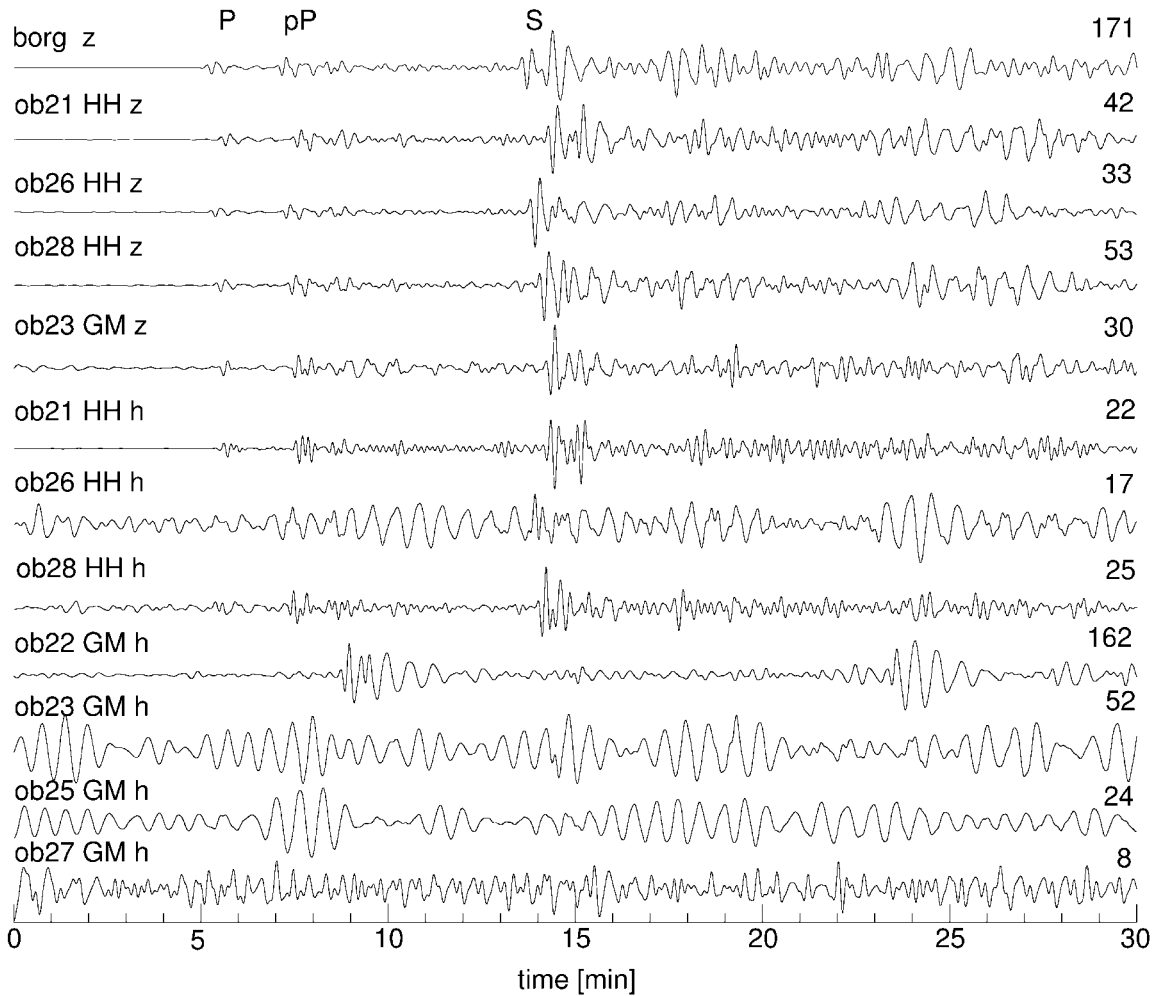


Figure 2. Recordings of the Kamchatka, 28 June 2002, M 7.3 event at the OBS stations deployed in the North Atlantic. BORG is the vertical channel of the permanent broadband station in Reykjavik, Iceland, and is plotted for comparison. The traces show available vertical and hydrophone channels indicated by z and h, respectively. Hamburg-type stations are indicated by HH, GEOMAR-type stations by GM. Traces have been deconvolved to displacement or quasi-displacement for hydrophones. A nine-pole Butterworth bandpass filter with corner frequencies at 0.025 and 0.1 Hz has been applied. Additional, tilt-induced long-period noise has been removed for ob26, ob28, and ob23. All traces are normalized to their own maxima, which are equal to 10^{-9} times the numbers in the upper right end of each trace. Station ob22 recorded the P wave, but the latter part of the wave train is affected by spikes (resulting in spurious signals in the bandpass-filtered record). The large low-frequency noise measured at DPG stations (ob23, ob25) is related to infragravity noise. It does not mean that DPGs are noisier than (piezoelectric) hydrophones, because the latter are not sensitive at these long periods and their true roll-off at 100 sec is unknown.

achieved by station ob21 (Fig. 4c). An equivalent technique for removing the effect of infragravity waves (Webb and Crawford, 1999), which makes use of the pressure signal to correct the vertical component, could not be applied in this case because none of the sites had both seismometers and pressure sensors with sufficient sensitivity in the infragravity band (here < 0.02 Hz). For further analysis, we applied the tilt correction to only those stations for which an improvement in SNR was achieved (ob06, ob08, ob23, ob26, ob28).

At the other stations (ob05, ob10, ob11, ob21) we continued to use the uncorrected signals.

Table 1 summarizes the estimated static sensor tilt on the seafloor for the stations deployed in the Tyrrhenian Sea and the North Atlantic. An apparent station tilt of $\Theta < 0.3^\circ$ was found to be small enough to avoid significant cross-over noise. Coherency between vertical and horizontal channels was then typically well below 0.5. This was the case for only two of the ten fully operational four-component stations of

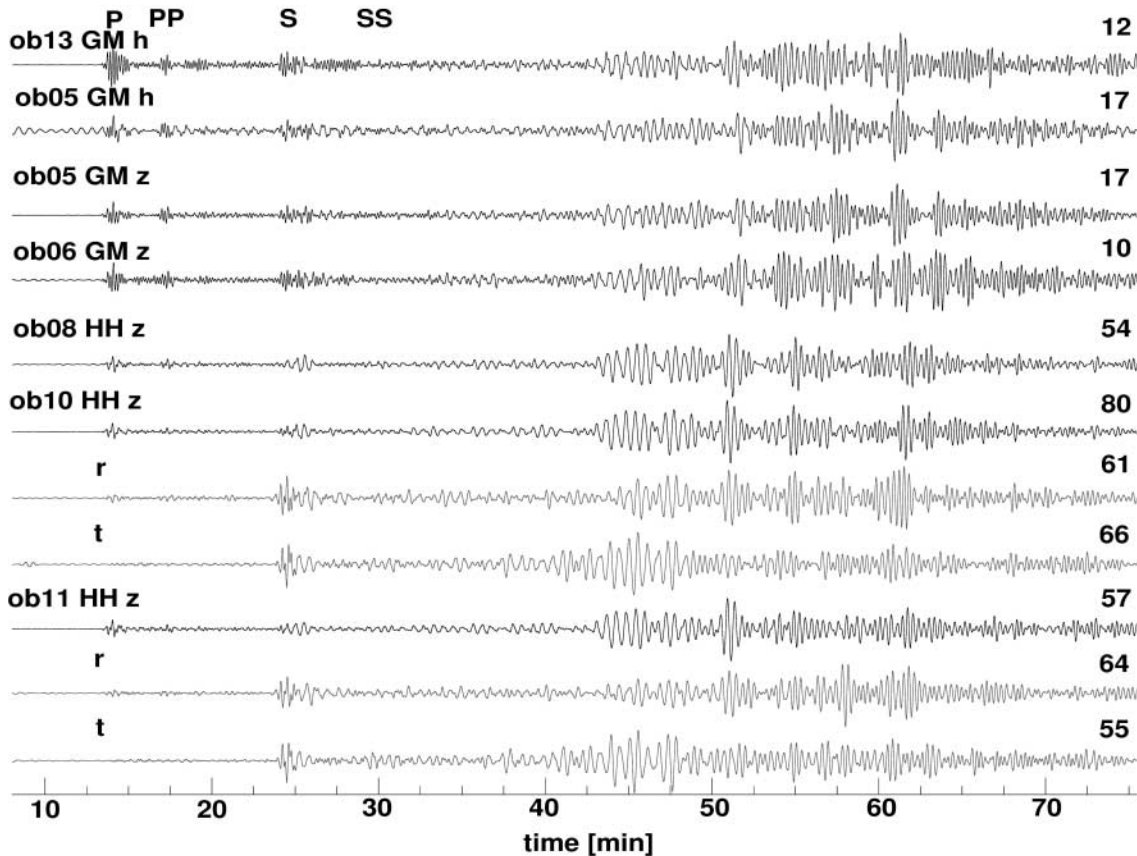


Figure 3. Recordings of the Kodiak Island, 10 January 2001, M 6.7 shallow event at the OBS stations deployed in the Tyrrhenian Sea. The epicentral distance was 84° . Vertical and hydrophone components are shown for the GEOMAR stations (top four traces). For the two Hamburg-type stations (ob10, ob11) three-component seismograms are shown, where the horizontal traces have been rotated to radial and transverse directions. The same normalization and filtering has been applied as in Figure 2.

the two deployments, which indicates that the leveling mechanism or the deployment technique is not satisfactory for either type of station. Hamburg-type stations (PMD seismometers) have passive gimbal systems where the seismic sensor is put in a highly viscous oil (10^5 Pa sec (at 20°C) for the Tyrrhenian Sea and 10^6 Pa sec for the North Atlantic). Assuming that the internal sensitivity axes of the PMD sensors are aligned at high precision, the observed misleveling of up to 7° at ob28 may have resulted from an imprecise weight balancing of the sensors in the pendulum mechanics. GEOMAR-type sensors (LDEO at ob05, ob06, ob23) are actively gimballed by a system developed by Webb *et al.* (2001). The small tilt angles of 0.3° and 0.7° at ob05 and ob23, respectively, indicate the *in situ* precision of the mechanics when the external pack is properly placed on the seafloor. In contrast, the extremely large value of 34° at ob06 would imply a strongly tilted external pack. However, the horizontal components could not work at such high tilt angles, so that the estimate for ob06 given in Table 1 cannot be taken at face value and probably indicates technical problems with the sensor.

The large tilt angles and the large tilt-induced vertical channel noise found at several of our free-fall stations show that the leveling mechanics as well as the deployment technique clearly have room for improvement. A more controlled launching of stations aided by video images of the seafloor might be preferential to the standard free-fall deployment technique to ensure a stable, approximately level placement of the stations on the seafloor. (The University of Hamburg recently successfully tested such a system during a deployment offshore Chile in February 2005).

Comparison of Noise Measurements

A standard procedure to quantify the fidelity of a seismic station is to compare PSDs with the low- and high-noise models of Peterson (1993), reflecting typical noise levels for good or poor permanent land stations. The PSD of background noise at our stations has been calculated by taking the median of the PSD of 1-hr intervals (mean-removed and instrument-deconvolved traces in m/sec^2 ; one-sided convention for PSD estimates), but excluding 3 hr after every earth-

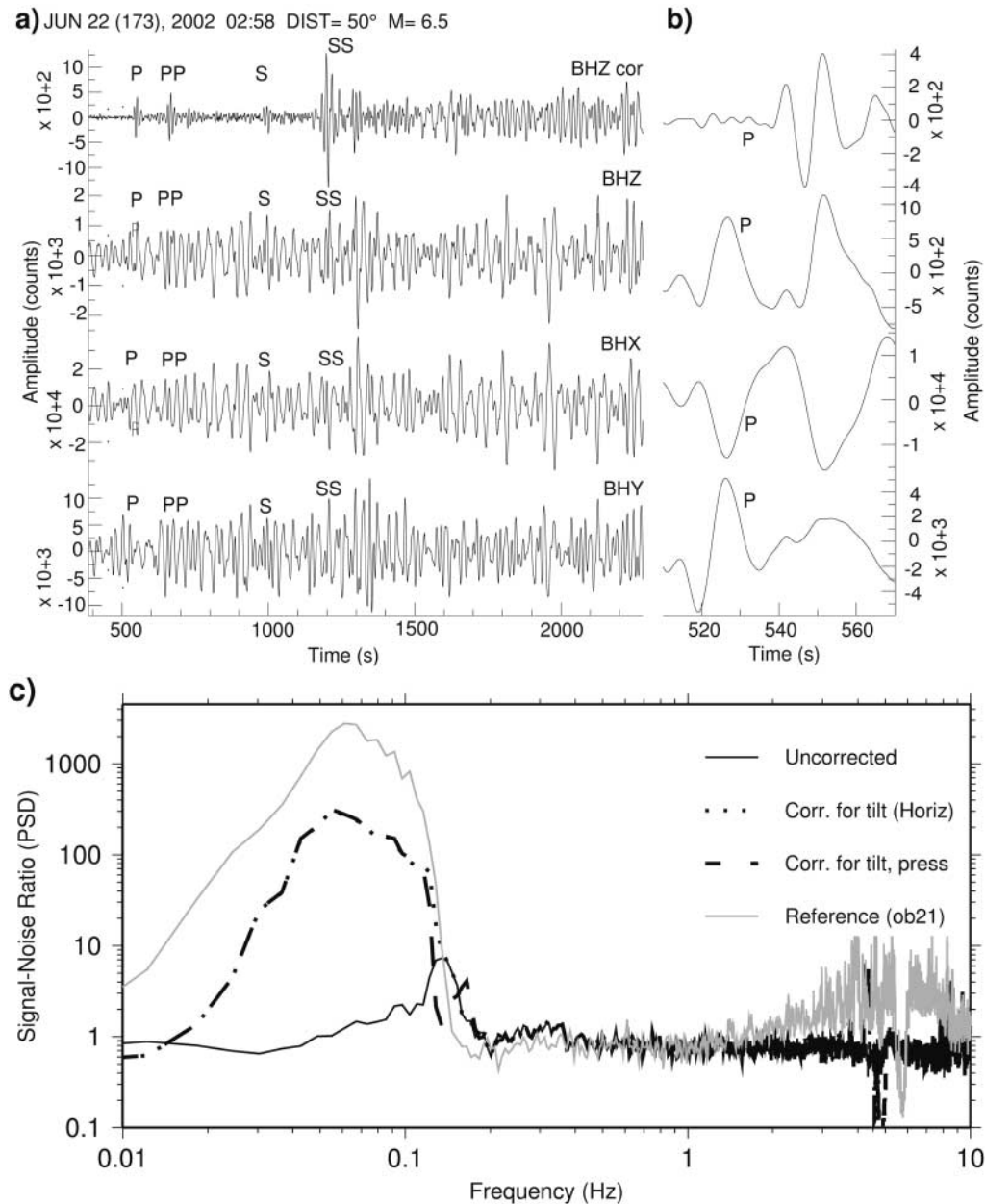


Figure 4. (a) Seismogram for a magnitude 6.5 event at 50° epicentral distance recorded by station ob28. The top trace shows the tilt-corrected vertical component, the second from the top trace shows the uncorrected vertical component, and the bottom traces show the two horizontal components. All traces are normalized to their own maxima and have been bandpass filtered with corners at 0.025 and 0.1 Hz. Note that the uncorrected vertical and horizontal waveforms are very similar, but the amplitude of the horizontal waveforms is much higher. (b) Magnification of the *P*-wave arrival for this event. (c) SNRs for corrected and uncorrected vertical channels of ob28 estimated from five events (at distances of 14°, 49°, 60°, 72°, and 112°). The SNR was estimated by using the PSDs for a window immediately preceding the event and a window encompassing the event (beginning with the *P*-wave arrival and including most of the surface-wave train). The SNR for station ob21 is included for reference (gray line). The actual value of the SNR is arbitrary because it depends on the events used, but the figure shows the significant improvement effected by the tilt-correction procedure.

Table 1

The Apparent Tilt-Angle Θ between the True Vertical (i.e., the Gradient of the Gravitational Potential) and the Vertical Sensitivity Axis of the Sensor and the Azimuth Angle φ between the Projection of the Tilted z Axis and the x Axis of the Sensor (Anticlockwise)

Tyrrhenian Sea Deployment 2000/2001					
	ob05	ob06	ob08	ob10	ob11
Θ (deg)	0.3 ± 0.6	(34 ± 7.1)	2.1 ± 0.2	1.2 ± 0.7	1.3 ± 0.3
φ (deg)	7 ± 4	(62 ± 4)	15 ± 1	137 ± 13	121 ± 8
North Atlantic Deployment 2002					
	ob21	ob23	ob26	ob28	
Θ (deg)	0.3 ± 0.2	0.7 ± 0.6	0.8 ± 0.2	7.1 ± 0.7	
φ (deg)	126 ± 8	231 ± 6	247 ± 12	64 ± 2	

Both angles have been averaged from the “flat” part of the transfer functions X/Z , Y/Z for $0.025 \text{ Hz} < f < 0.08 \text{ Hz}$. Values in parentheses cannot be interpreted as true station tilt but more likely reflect other instrumental problems, for example, with the gain of internal amplifiers.

quake with $M \geq 5.5$. Figure 5 compares the median vertical component PSD of the two deployments to the noise models of Peterson (1993); below 0.1 Hz the tilt-induced noise has been reduced for ob08, ob23, ob26, and ob28 by the technique described in the appendix. Figure 6 shows the median PSD estimate of pressure for the North Atlantic. The PSDs are characterized by three noise intervals: the so-called “low-noise notch” between 0.01 and 0.1 Hz (e.g., Webb, 1998), the microseismic noise between 0.1 and about 1 Hz, and the high-frequency noise above 1 Hz. The stations with the lowest noise levels in the frequency range between 0.01 and 0.1 Hz have a PSD of $10^{-15} \text{ m}^2/\text{sec}^4/\text{Hz}$, about 30 dB above the noise level of quiet stations of the low-noise model of

Peterson (1993). We believe that the noise level of $10^{-15} \text{ m}^2/\text{sec}^4/\text{Hz}$ at 0.05 Hz is nearly the optimum for the free-fall stations used and is apparently independent of the region, because this level is nearly the same for the North Atlantic and Tyrrhenian Sea deployments.

The microseismic noise peak at 0.24 Hz has a maximum of about $10^{-9} \text{ m}^2/\text{sec}^4/\text{Hz}$ in the North Atlantic and about $10^{-11} \text{ m}^2/\text{sec}^4/\text{Hz}$ in the Tyrrhenian Sea. It is the most dominant signal below 5 Hz in both cases. The differences between the two deployments reflect differences in the strength of the noise sources and, maybe to a larger part, differences in source-station distances. The microseismic noise measured in the North Atlantic is partly above the level of noisy oceanic island stations of Peterson’s high-noise model.

The noise peaks above 2 Hz are interpreted as local site resonances and shear-wave resonances as proposed by Godin and Chapman (1999). Local and regional earthquakes have not been systematically removed from the analysis, but because we are calculating the median they should not influence the noise level significantly. The pronounced high-frequency peaks are very different for the same instruments at different sites and are therefore not related to the instrument or leveling system.

Table 2 gives measured average noise levels on horizontal channels in the frequency band from 0.05 to 0.1 Hz. See Figure 15 for examples of PSDs of horizontal channels. The lowest level is at about $10^{-13} \text{ m}^2/\text{s}^4/\text{Hz}$ and thus a factor of 100 larger than the lowest level on vertical channels (factor of 10 in amplitudes).

The higher low-frequency noise level on horizontal channels is commonly observed on the seafloor and associated with current-induced tilt transients experienced by the sensor. Duennebieer and Sutton (1995) and Crawford and

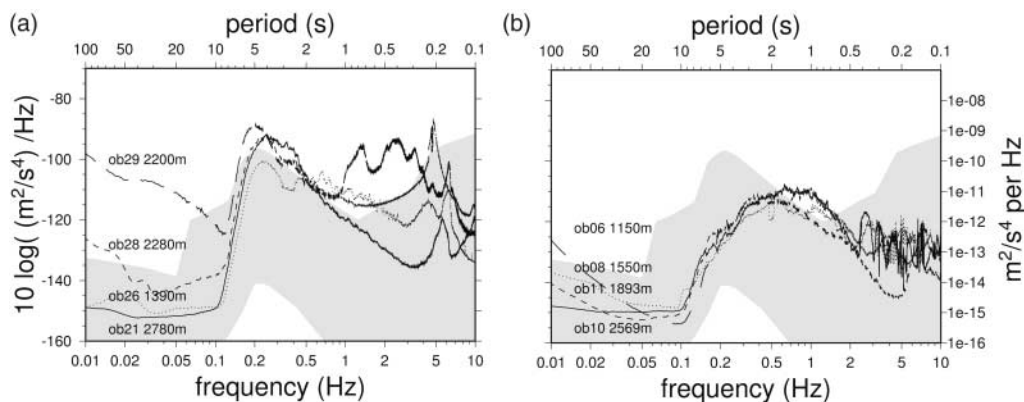


Figure 5. The median vertical PSD of OBS stations deployed in the North Atlantic (a) and Tyrrhenian Sea (b), where a time window of 85 (julian day from 104 to 189) and 146 days (day 337 in 2000 to 117 in 2001) has been used. Teleseismic earthquake signals ($M > 6$) have been removed from the analysis. Sensors ob29 and ob06 had an unknown amplification factor and their median PSD curves were therefore scaled to fit the microseismic peaks of nearby calibrated stations (see Figs. 7b and 8b). Tilt-induced noise has been corrected below 0.1 Hz for ob06, ob08, ob26, and ob28. The range between the USGS low- and high-noise models (Peterson, 1993) is indicated by gray shading. The deployment depth is indicated in meters.

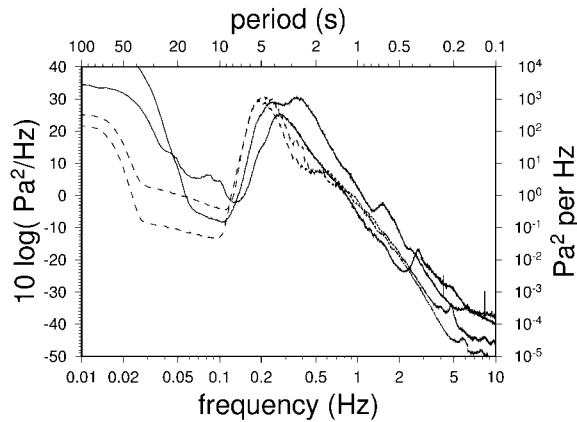


Figure 6. The median PSD of differential pressure gauges (ob23, ob25; continuous lines) and hydrophones (ob27, ob28; dashed lines) in the North Atlantic. Note that the noise level in the infragravity band should be similar for all pressure sensors. The differences below 0.1 Hz possibly reflect unknown differences between sensors or wrong corrections of roll-offs at very long periods.

Webb (2000) give the equations to estimate vertical and horizontal channel noise resulting from a harmonic tilt excitation with amplitude ε , frequency ω , dependent on the following station parameters: distance L of the sensor to the center of rotation and various angles describing the permanent tilt of the sensor and its position relative to the center of rotation. At low frequencies, the tilt amplitude on the horizontal channels is to first-order proportional to ε . If the center of rotation is far from the sensor, an additional term proportional to $\varepsilon\omega^2L$ becomes important at high frequencies. A station or an instrument pack with a larger flow-resistance torque will generate larger current-induced tilt. Further, the anchor of the station (instrument pack) will be important, because it has to couple to the ground without wobbling and needs ground-contact points spread over as large a distance as possible, compared with station or package height.

An interesting question is how variable the noise on horizontal channels is and whether a systematic effect can be seen depending in the station type, that is, external pack (GEOMAR-type) compared with station-integrated sensor (Hamburg-type). In general, the stations with the smallest noise on horizontal channels were also the stations characterized by the highest fidelity of the vertical channels (ob10, ob11, ob21). Horizontal noise levels of the problematic Hamburg-type stations (ob08, ob28) were more than 30 dB higher than those of the high-fidelity stations. Ob28 had a compliant frame built from glass-fiber-reinforced plastic (GRP), which might have added to an enhanced tilt signal at this stations. Otherwise, the increased tilt noise on horizontal channels is most likely related to a very soft seafloor site or an unlucky deployment with a wobbling station. There appears to be a tendency for GEOMAR-type stations with external packs (ob05, ob06, ob23, and ob29) to have higher

Table 2

Average PSD Noise for $0.05 < f < 0.1$ Hz on Horizontal Channels x and y in $10^{-12}/\text{m}^2/\text{sec}^4/\text{Hz}$.

Tyrrhenian Sea Deployment 2000/2001					
	ob05	ob06	ob08	ob10	ob11
x	2162	1148	108	2	0.1
y	2412	1300	1414	2	0.3
North Atlantic Deployment 2002					
	ob21	ob23	ob26	ob28	
x	2	7000	194	1668	
y	3	4400	111	335	

noise levels than Hamburg-type stations with integrated sensors, again with noise levels about 30 dB higher than at the high-fidelity stations. This might indicate that at low frequencies the external pack was more sensitive to bottom currents than the other stations, although an unlucky, wobbling deployment site is a second possible explanation.

To quantify the noise level for the whole deployment period the PSD of seismic records has been analyzed as a function of time. For a 3-hr sampling interval and 6-hr overlapping time windows, traces have been mean removed, deconvolved to velocity (by adding one zero to the pole-zero file for acceleration) and bandpass filtered with Gaussian filters centered at $f_0 = 0.06, 0.12, 0.24, 0.48, 0.96,$ and 1.92 Hz and with a one-octave bandwidth (the transfer function is $H = e^{-\alpha(\omega - \omega_0)^2/\omega_0}$ with $\alpha = 3.5/b^2$, $b = 1/3$ and is non-zero between $2/3 f_0$ and $4/3 f_0$ only). Then, the PSD was calculated, low-pass filtered, and resampled before plotting in logarithmic scale. For detailed analysis, three center frequencies have been selected for three Hamburg-type stations deployed in the Tyrrhenian Sea (Fig. 7) and the North Atlantic (Fig. 8). The PSD for $f_0 = 0.06$ Hz represents the low-noise notch below the microseismic noise peak, the PSD for $f_0 = 0.24$ Hz samples the oceanic wave-generated microseismic noise, whereas $f_0 = 1.92$ Hz lies above the classical microseismic peak. For teleseismic seismological studies the frequency range from 0.01 to 2 Hz is of most interest.

The two lower traces in the low-noise notch passband in Figure 7a (Tyrrhenian Sea deployment, ob10 and ob11 at 0.06 Hz) show the expected behavior; the background noise level is relatively small and clearly exceeded by signals of teleseismic earthquakes (narrow peaks). The earthquake peaks can be associated with surface-wave energy. Thus, Figure 7a gives the possibility to quantify and compare detection thresholds for surface waves. $M \geq 7$ events exceed the noise level by nearly 50 dB, and $M \geq 5.8$ events still exceed the noise level by about 20 dB.

Station ob08 was characterized by relatively large long-period noise on the horizontal components. Although the traces have been tilt corrected by the technique described previously, the vertical background noise is still enhanced at ob08 (Fig. 7a, upper trace). We believe that most of this

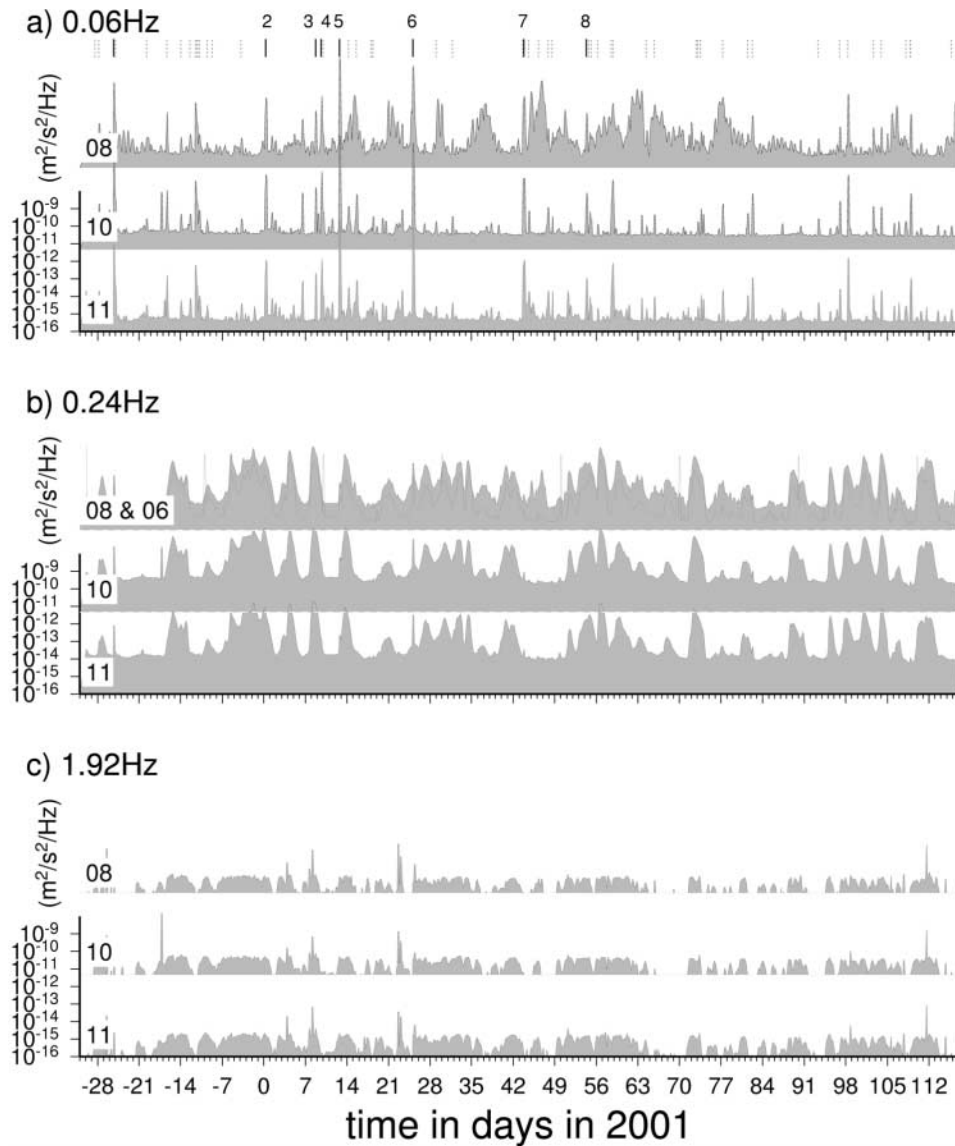


Figure 7. Power spectral density for ground velocity (PSD) in 6-hr overlapping time windows at three Hamburg-type stations deployed in the Tyrrhenian Sea (vertical seismometer channel). (a) PSD for the “noise notch” frequency band around $f_0 = 0.06$ Hz. (b) PSD for the microseismic frequency band centered at $f_0 = 0.24$ Hz. (c) PSD for the high-frequency microseismic noise band centered at $f_0 = 1.9$ Hz. In b, the PSD of the nearby station ob06 (vertical component, Webb-Sensor) is compared with that of ob08 (shifted a constant factor of 0.25 downward). The deployment depths were 1550, 1893, and 2569 m for ob08, ob11, and ob10, respectively. Occurrence times of teleseismic earthquakes with $M > 5.8$ are indicated by marker lines in a, where numbers indicate earthquakes with $M \geq 7$.

low-frequency noise was current induced. Because ob08 was technically identical with ob10 and ob11, the enhanced noise at ob08 indicates local current variations or that the station landed in an unstable position on the seafloor.

In the 0.24-Hz passband the microseismic noise is the dominant signal for all three stations (Fig. 7b; the PSD is a factor of approximately 4 larger than for 0.06 Hz). Single, isolated noise events are visible as broad peaks and can be associated with single “storms” or “high-swell events” in the

Mediterranean Sea or the Atlantic. A noise peak may cover a range of 40 dB on the vertical channels. Because the absolute noise level is increased compared with the low-noise notch, signals from $M \geq 7$ earthquakes are detectable in only a few cases (e.g., events 1 and 6). The microseismic noise is very similar and correlated between the stations, which were 30 and 40 km apart.

In the 1.92-Hz passband (Fig. 7c) the background noise of ground velocity power is smaller again (by a factor of 0.1

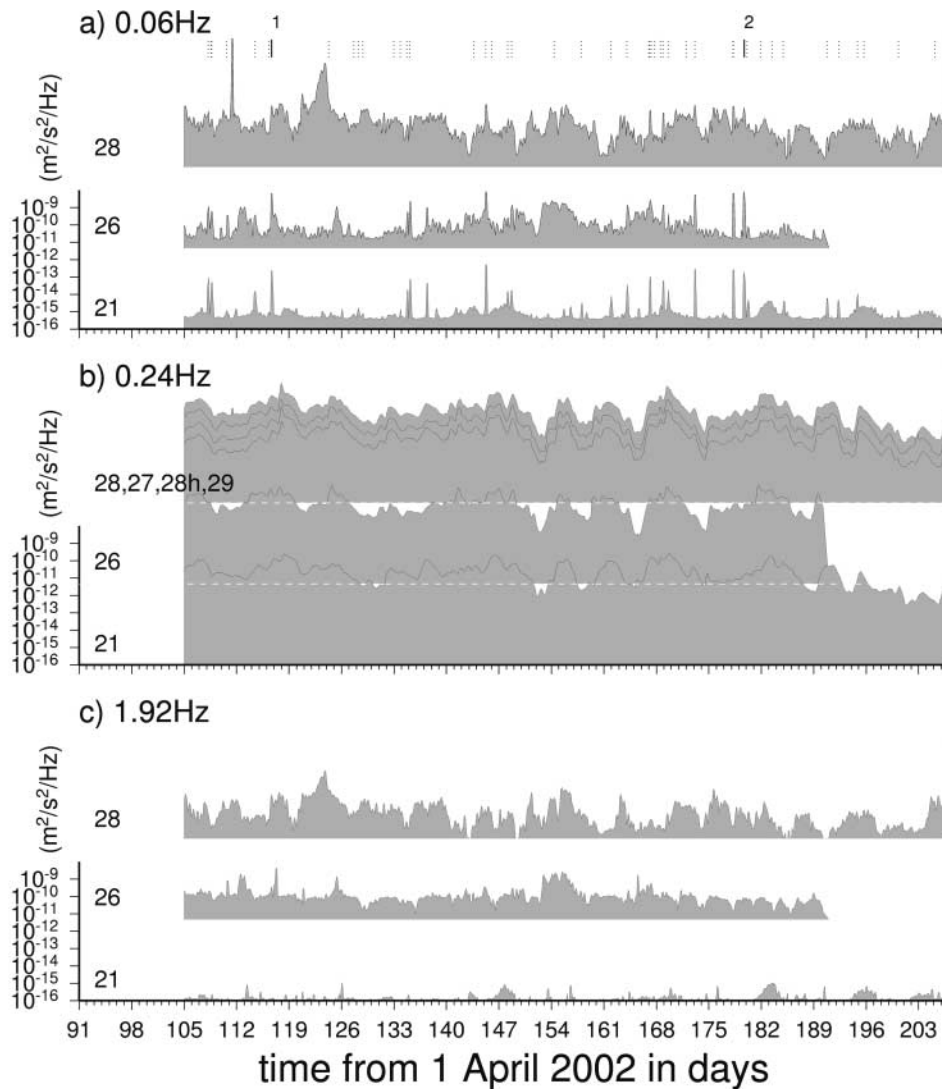


Figure 8. Ground-velocity PSD at three Hamburg-type stations deployed in the North Atlantic. In b, the PSD of nearby stations ob27 and ob28 (hydrophone converted to quasi-velocity) and ob29 (z , PMD, only until day 119) are compared with the vertical component of ob28 (shifted a constant factor of 0.25 each). The station depths for stations ob21, ob26, and ob28 are 2780, 1389, and 2268 m, respectively. See Figure 7 for further explanations.

compared with the 0.06 Hz noise). Nevertheless, signals from teleseismic earthquakes are often not detectable because of attenuation along their travel path and because large earthquakes have limits on the radiation of high-frequency energy. However, regional and local earthquake signals are apparent in Figure 7c as correlated narrow peaks. The noise levels follow a clear pattern and appear to be correlated between the three stations. Discarding the earthquake-related peaks, the 1.92-Hz traces have flat ceilings. Troughs in the curves are often but not always associated with troughs in the 0.24-Hz band. McCreery *et al.* (1993) observed similar flat tops on hydrophone records in the Pacific and explain them as saturation of the ocean-wave spectrum for strong winds, resulting in the so-called Holu spectrum.

Figure 8 shows the same analysis for the North Atlantic and the deployment in 2002. The three Hamburg-type stations have a design and sensors identical with those of the Tyrrhenian Sea experiment. In Figure 8a only the data of ob21 are of comparable quality to those recorded in the Tyrrhenian Sea. Signals from $M \geq 6$ earthquakes are well detected in the low-noise frequency band centered at 0.06 Hz. As discussed previously, the enhanced noise levels for stations ob26 and ob28 again reflect current-induced noise transferred to the vertical because of sensor misalignment.

The microseismic noise levels (Fig. 8b) appear again highly correlated, although the stations have been up to 400 km apart. In contrast to the observation in the Tyrrhenian Sea, the storm peaks are not isolated and strong micro-

seismic noise seems to be continuously excited. The absolute noise level is also higher than in the Tyrrhenian Sea, so that even the M 7.3 earthquake is barely visible in this frequency range. This observation is confirmed by Figure 15c, which shows that the SNR of earthquake data has been about 1 in the North Atlantic for frequencies above 0.1 Hz.

The absolute noise level in the North Atlantic at 1.92 Hz is comparable to that in the Tyrrhenian Sea. Only few local and regional “earthquake peaks” show up in Figure 8c. Instead of a flat ceiling as in the Tyrrhenian Sea, a flat level is observed for ob21 and ob26 with excursions in both directions. The noise levels are not correlated with the noise at 0.24 Hz. In contrast to the Tyrrhenian Sea, the 1.92-Hz noise levels are also not correlated between the stations. This indicates distinct generation areas for each station, with an extent less than the smallest interstation distance (≈ 150 km). We demonstrate subsequently that the noise at about 1 Hz is predominantly generated by local oceanic waves above the station, whereas the larger noise at 0.24 Hz stems predominantly from regional or even teleseismic source areas.

We now address the question of whether a brief transient signal, for example, a P -wave arrival, can be detected in a narrow-frequency band against a background of continuous noise. Because the P wave has a finite energy and hence zero power when averaged over all time, we follow Webb (1998) by comparing the root-mean-square noise in a given frequency band ($\sqrt{\text{PSD}(f_0)} f_0 \Delta f$, where $\Delta f = 2^{1/6} - 2^{-1/6}$ is the 1/3-octave relative bandwidth) with model amplitudes of P waves in that band (Fig. 9). The three noise curves represent the first quartile, median, and third quartile as estimated from the whole deployment period (earthquakes removed) and the high-fidelity stations (ob10 and ob21). To calculate model amplitudes of body waves at teleseismic distances we follow the procedure described in the appendix of

Webb (1998), where a shallow earthquake at 70° epicentral distance and an attenuation parameter $t^* = 1$ sec has been assumed. Higher values of t^* would strongly reduce amplitudes at higher frequencies (see Webb [1998] for comparison and discussion). For tomography one would like to analyze the teleseismic body waves at frequencies as high as possible. However, a typical range is between 0.02 and 2 Hz. Body-wave arrivals can most likely be detected and analyzed when their signal amplitude exceeds the noise amplitude by a factor of about 6 (16 dB). Assuming that the several-month deployments are representative for a whole year, detection probabilities can be derived from Figure 9 and are discussed for distinct frequencies. The intersections of the first-, second-, and third-quartile noise curves, adjusted upward by the required SNR (here 16 db), with the curves for predicted amplitudes of different magnitude earthquakes give the detection thresholds for 25%, 50%, and 75% detection probability, respectively. We only plot predicted amplitudes for increments of 1 magnitude unit and obtain intermediate magnitudes by interpolation between these curves.

At 0.1 Hz and for the best stations, the body wave from a M_w 6 event at about 70° distance can be detected with a probability of about 75% for both the North Atlantic and the Tyrrhenian Sea. Large differences occur at 0.25 Hz. In the Tyrrhenian Sea, the probabilities to see a M_w 6.8, 6.2, and 5.8 event are about 75%, 50%, and 25%, respectively, whereas in the North Atlantic, basically no teleseismic earthquake is expected to be detected (the 50% probability detection threshold exceeds M_w 8.0). At 1 Hz, the North Atlantic is apparently quieter than the Tyrrhenian Sea, and a M_w 6.0 event would be detected during about 50% of the deployment days. However, the prediction error of earthquake amplitudes is relatively large at 1 Hz so that estimates are more uncertain. The detection threshold at frequencies

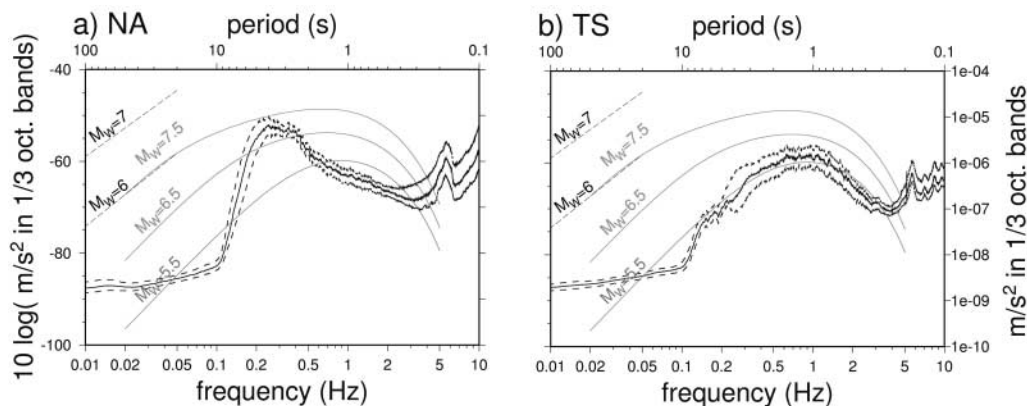


Figure 9. Models of the vertical acceleration amplitudes in 1/3 octave bands of surface waves (dashed) and P waves (continuous) from earthquakes at a distance of 70° and an assumed frequency-independent attenuation parameter $t^* = 1$ sec (see Webb [1998] for further description). Also shown are the first quartile, median, and third quartile of vertical acceleration noise ($a_{\text{rms}} = \sqrt{\text{PSD}(f_0)} f_0 (2^{1/6} - 2^{-1/6})$) at the highest-fidelity stations in the North Atlantic (NA) [(a); ob21] and Tyrrhenian Sea (TS) [(b); ob10]. Windows containing large earthquakes have been removed from data streams.

above 1 Hz is even more difficult to estimate because body-wave amplitudes are more variable there, depending on t^* and other factors. Assuming that a SNR of 20 dB is required for analysis of surface-wave dispersion, surface waves at 0.05 Hz from a M_w 6.1 earthquake at 70° distance would be observed 75% of the time on the vertical components of our high-fidelity stations in both the North Atlantic and the Tyrrhenian Sea.

The noise level measured at sites on the East Pacific Rise (see figure 2 of Webb, 1998) is slightly higher than that observed in the North Atlantic.

In Figure 10, the pressure noise is compared with body-wave model amplitudes. The amplitudes of the theoretical pressure signals in the water have been calculated by multiplying the vertical particle velocity by $1000 \text{ kg/m}^3 \cdot 1500 \text{ m/sec}$. In the North Atlantic, the probability to detect a M_w 7.5 event (70°) with a hydrophone at frequencies above 0.2 Hz is clearly less than 25%. The high-frequency boundary for the 25% probability is shifted to about 1 Hz in the Tyrrhenian Sea.

The estimates of Figures 9 and 10 agree well with our experience when looking at the data and the general picture derived from Figures 7 and 8. However, the detection threshold at low frequencies can be increased by unfavorable site conditions by up to one magnitude step (for corrected vertical components).

Oceanic Gravity Waves and Noise Generation

Microseismic noise between 0.1 and 1 Hz is generated by oceanic gravity waves coupling some of their energy to the seafloor and thereby exciting elastic waves. Microseismic noise on land stations travels predominantly as Rayleigh waves and can be observed far from its generation areas (Essen *et al.*, 2003).

Figure 11 shows the average annual waveheight of oce-

anic gravity waves in 2002 calculated from global oceanic wave models (WAM; e.g., Komen *et al.*, 1994) which sample the sea waveheight in 6-hr intervals and 1° grid spacing. The largest oceanic waves, and thus the largest microseismic noise, can be expected south of 45° S. Noise conditions should be optimal in the equatorial regions. In the North Atlantic and North Pacific the noise level is expected to be significantly lower during the summer, because average height of long-period oceanic waves is lower during the summer. The figure shows that the expected noise is much lower at the Galapagos hotspot, the Seychelles, or Cape Verde that at Iceland or off-shore South Chile. The Mediterranean Sea and especially the Aegean Sea should have one of the lowest microseismic noise levels.

The observed noise and the estimated detection thresholds in the North Atlantic and the Tyrrhenian Sea correlate well with the average oceanic waveheights in Figure 11. South of Iceland in the North Atlantic the average annual waveheight is about 3 m. It is only half a meter or less in the Tyrrhenian Sea. Thus, a comparative approach can be used to roughly predict expected detection thresholds in other regions of the world's oceans; for example, latitudes below 42° S have the largest average waveheights of 4 m and more and are thus expected to have the worst microseismic noise.

The WAM model waveheights of the North Atlantic were calculated by the Deutsche Wetterdienst in Offenbach, Germany, and have been sampled at 3-hr intervals and 0.75° grid spacing. To locate the generation areas of microseismic noise in the North Atlantic we correlate the WAM oceanic waveheight with the square-root of PSD time series for different passbands, as plotted in Figures 7 and 8. For example, the 1-Hz vertical channel noise at ob21 correlates well with the sea waveheights directly above the station (Fig. 12), whereas the noise at 0.24 Hz does not, even though it is ~ 100 times stronger. We assume that a good correlation of

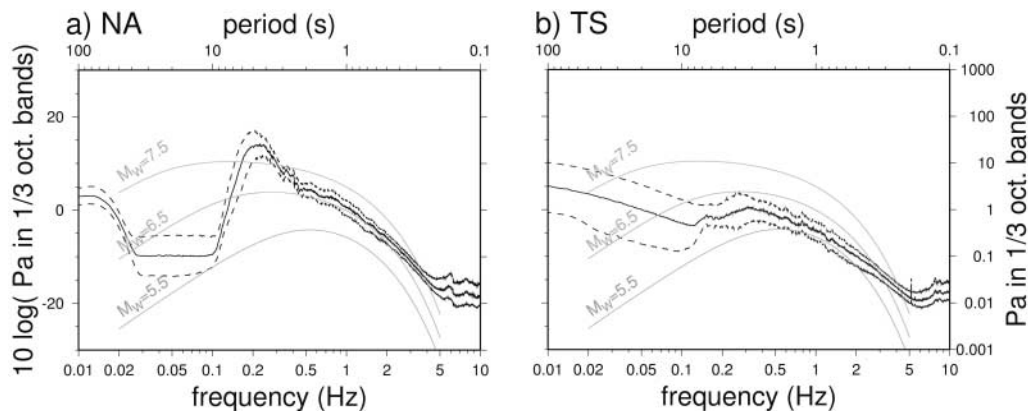


Figure 10. Models of the amplitudes in pressure in 1/3 octave bands of the teleseismic P waves (70°) are compared with first quartile, median, and third quartile of pressure noise in the North Atlantic (NA) [(a); ob21] and Tyrrhenian Sea (TS) [(b); ob10]. See Figure 9 for further description.

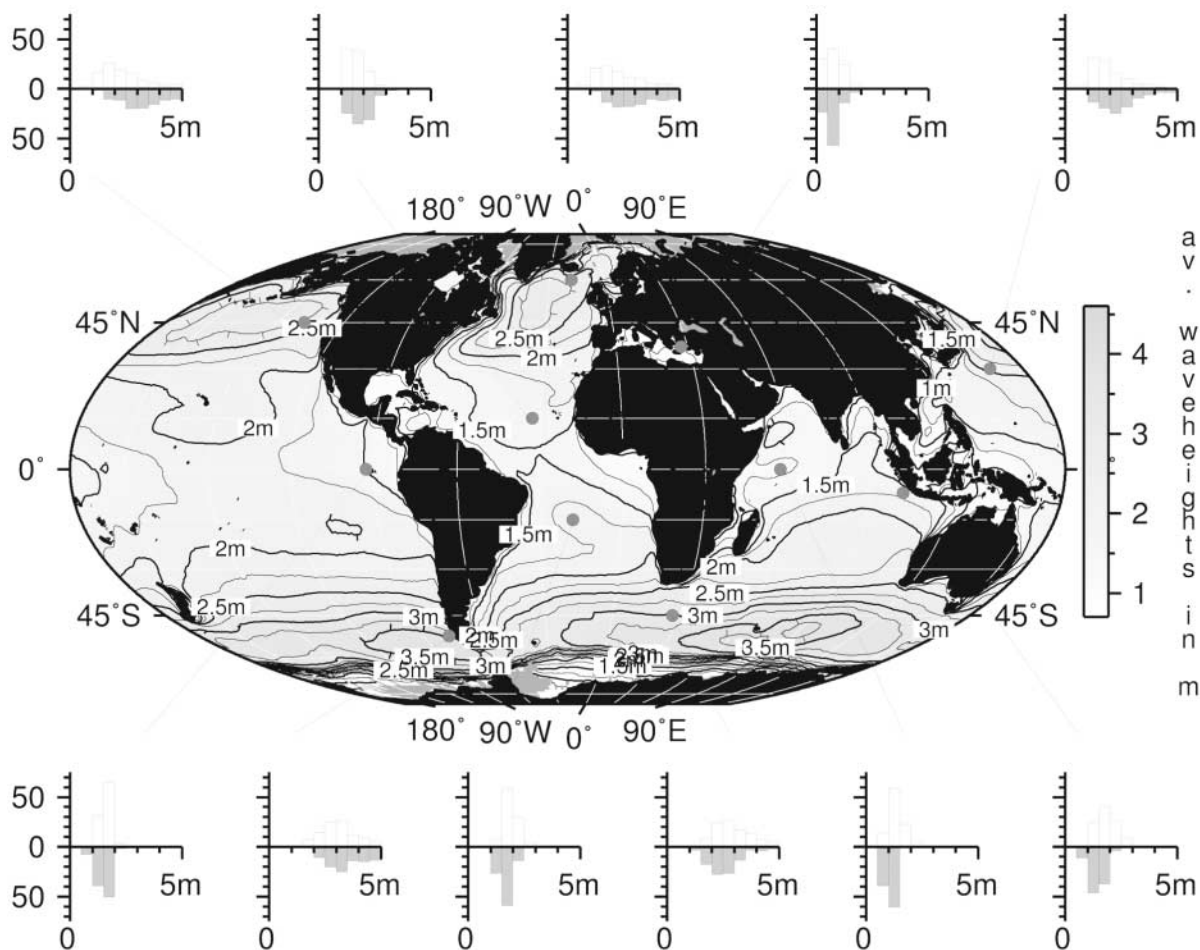


Figure 11. Average oceanic waveheight in 2002. Histograms show the frequency of occurrence of waveheights for selected locations (open circles), where the upper histograms (white) correspond to the period from April to September, and the lower histograms (gray) from October to March, respectively.

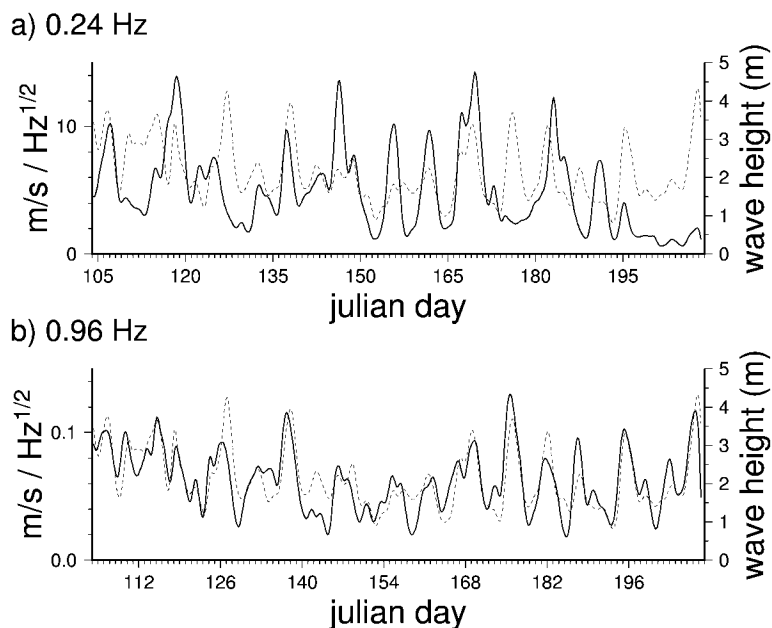


Figure 12. Comparison of seismic seafloor noise (continuous line, square root of noise PSD) and oceanic waveheight (dashed line) at the position of ob21. A Gauss filter center frequency of 0.24 and 0.96 Hz has been applied to the seismic data in (a) and (b), respectively.

oceanic waveheights and noise PSD, more precisely its square root, over the recording period of 3.5 months indicates a major noise generation area. This assumption is justified when the major noise generation areas for seismic noise at a given station remain the same throughout the experiment. Thus, Figure 12 indicates that most of the secondary microseismic noise at ob21 is not generated locally.

To estimate the major generation areas of noise at ob21 we calculated and plotted linear correlation coefficients between the measured noise on the vertical channel and sea waveheights (Fig. 13; both time series are smoothed with a 48-hr running average filter). This correlation technique has been applied successfully on land stations to estimate generation areas of secondary microseismic noise in North Europe (Essen *et al.*, 2003). We find that the secondary microseismic noise at ob21 was mainly generated off-coast of Ireland and Scotland (Fig. 13a), whereas the noise at 1 Hz was indeed generated by oceanic waves above the station. This observation is of interest because it predicts that a large portion of the noise signals at 0.24 Hz are likely to arrive as plane waves at the station and may therefore be attenuated by applying array methods if a suitable station configuration is employed.

Applying the same analysis to the other deployed stations showed partly similar patterns but also revealed further generation areas. For instance, ob24 has the highest correlation coefficient to a source region on the Mid-Atlantic Ridge (MAR) off-coast South Iceland, whereas oceanic waves off the coast of Ireland seem to have a minor influence. To estimate all source regions of secondary microseismic noise relevant for the complete OBS array we calculated an average noise PSD time series before correlating with oceanic waveheights: Figure 14a indicates that altogether three major noise generation areas are effective, one off-coast West Ireland, the second off-coast South Iceland on the MAR, and the third in a band northeast of Iceland. The correlation coefficient is largest for the region off-coast

Ireland, indicating that this is the strongest generation area among the three.

Knowing the major generation areas of noise before a deployment can help to optimize the array and network design. Figure 14b shows that the major generation areas can be roughly estimated when averaging PSD noise curves from inland stations and correlation with WAM waveheights. In our case station BORG on Iceland and ESK on Scotland have been used for averaging. More stations may be added, although our tests showed that adding stations will not significantly change the pattern in Figure 14b.

Discussion and Conclusion

We have analyzed data from long-term deployments in the Tyrrhenian Sea and in the North Atlantic to characterize the seafloor broadband noise and the differences between two types of free-fall ocean-bottom stations. Free-fall broadband OBS have been proposed to be used for several large-scale passive seismological experiments. Therefore, our results and analysis are of interest to better plan these experiments and deployments and to improve the station design, the array configuration, and the deployment technique.

The Role of the Station Design and Current-Induced Noise

Similarly to observations with other broadband OBS our free-fall stations experience the lowest noise in the low-noise notch below 0.1 Hz. The low-noise notch is bounded by the microseismic noise at high frequencies and by noise from infragravity waves at low frequencies, which depends on the water depth. The low-noise notch is of interest for surface-wave and teleseismic long-period body-wave studies. It is likely that the noise level in the low-noise notch is determined by current-induced tilt. The ocean seismic network pilot experiment (OSNP) and MOISE experiment confirm

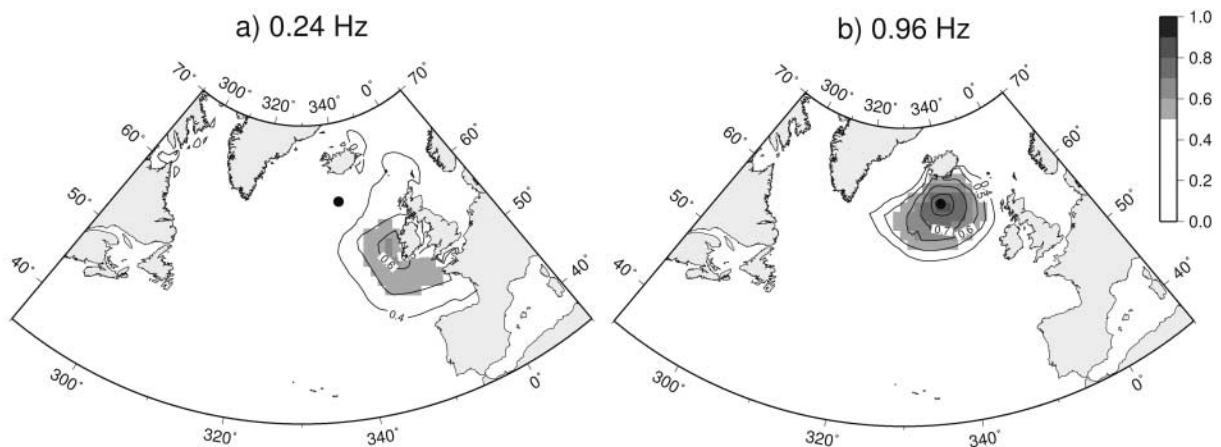


Figure 13. Linear correlation coefficient between the oceanic waveheight field and the power of filtered vertical ground velocity at station ob21 (filled circle) bandpass filtered at $f_0 = 0.24$ Hz (a) and 0.96 Hz (b).

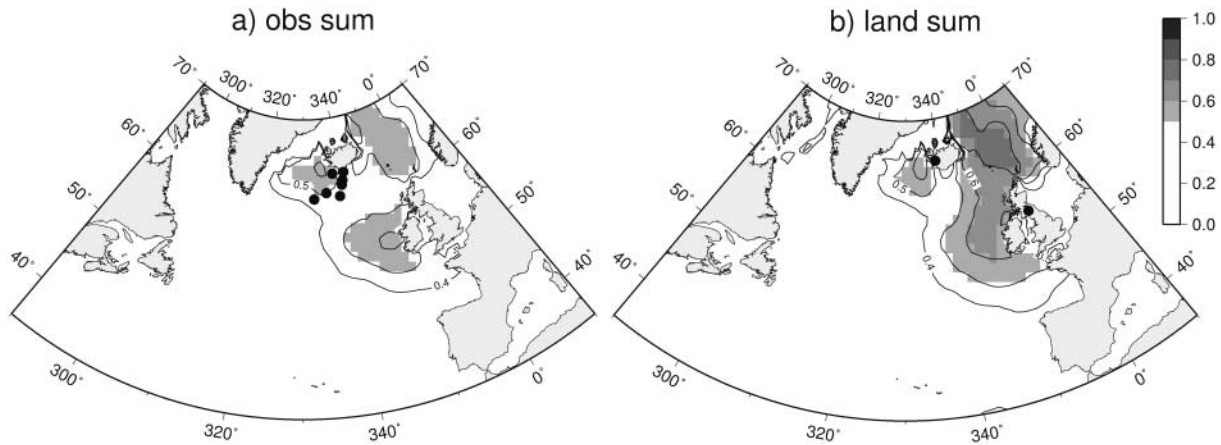


Figure 14. Superposed correlation coefficients from all OBS stations deployed (a) and from the two land stations BORG and ESK for comparison (b). The station locations are indicated by filled circles. The bandpass filter had a center frequency at the secondary microseismic noise peak ($f_0 = 0.24$ Hz).

this view (Collins *et al.*, 2001; Stutzmann *et al.*, 2001; Stephen *et al.*, 2003). Three broadband seismographs have been deployed close to the ODP Hole 843B at 4400 m depth located about 225 km southwest of Oahu, Hawaii. One was deployed in a borehole 240 m beneath the seafloor, a second was buried just below the seafloor, and a third was placed on the seafloor. Below 0.1 Hz the sensor buried under the seafloor was tens of decibels quieter than the one sitting on the seafloor. The noise level of the station sitting on the seafloor was correlated with current speed and increased with current speed by about 8 dB/cm/sec on the horizontal component.

For our high-fidelity stations the median noise level in the low-noise notch at 0.08 Hz was about 10^{-15} and 10^{-13} $\text{m}^2/\text{sec}^4/\text{Hz}$ on the vertical and horizontal seismometer channels, respectively, and thus comparable or slightly worse than “quiet day” measurements of the broadband seafloor station of the OSNP experiment, which showed values at this frequency of about 10^{-16} and $10^{-13.5}$ $\text{m}^2/\text{sec}^4/\text{Hz}$ (see Stephen *et al.*, 2003). The current-induced noise depends strongly on the deployment site, for example, whether the station is deployed on a steep slope or in a sea-bottom bathymetric valley. However, the differences in noise level by a factor up to 1000 and more in noise level at the different stations may also indicate differences in station design that determine susceptibility to currents or promote “wobbling.” For instance, the deployment of an external pack is recommended by many seismologists to reduce noise from a possible vibration of the station frame. However, from the long-term deployments with different stations types we can conclude that stations with external packs have never achieved a lower horizontal low-frequency noise level than those with a frame-integrated sensor. At the same time, the frame-integrated stations are easier to handle and less sensitive to mechanical malfunction. Another noise problem we identified is the wobbling of single stations for unlucky sta-

tion sites due to the uncontrolled nature of free-fall deployments. This suggests that a more controlled launching with video support has the potential to further reduce the current-induced noise.

The current-induced tilt noise is mainly felt by horizontal sensors. However, if the sensor is badly leveled the horizontal tilt noise is transferred to the vertical channel. We have estimated misalignments of several degrees (up to 7°). In conclusion, further improving leveling mechanics will significantly reduce cross-coupling and thus low-frequency noise on the vertical channels.

In addition, we were able to demonstrate that tilt-induced noise on the vertical component can be efficiently reduced when horizontal seismometer data are available. The increase in SNR for amplitudes was about a factor of 200 or more at noisy stations, showing the importance of measuring with three-component seismometers.

Character and Generation of Microseismic Seafloor Noise

Narrowband microseisms with a peak frequency at about 0.24 Hz are the dominant source of noise recorded on our free-fall OBS. They strongly depend on the experiment region. For example, in the North Atlantic the microseismic noise power is about a factor of at least 100 larger than in the Tyrrhenian Sea. The large amplitudes and the frequencies of the microseismic noise can be explained by a nonlinear fluid-dynamic effect in the oceanic layer, when standing oceanic gravity waves pressurize the seafloor at twice the frequency of the oceanic waves, which have their largest amplitudes at about 0.12 Hz (the spectrum of water waves depends on different factors and waves are dispersive). By analyzing land stations, Essen *et al.* (2003) have shown that most of the secondary microseismic noise in the North Atlantic is generated at a few sites near the coasts of Norway

and Scotland. This result is further confirmed and extended by our study. We identify additional generation areas of microseismic noise for the North Atlantic off-shore the north-west coast of Ireland/Scotland, on the Reykjanes Ridge south of Iceland, and in a band between North Iceland and West Norway. The generation areas are dominant presumably because the submarine topography and the preferential wind-wave directions are particularly favorable toward conversion of oceanic wave energy into secondary microseisms.

By using the same technique, similar generation areas were found for the microseismic noise on the land stations closest to our OBS array (BORG and ESK). This means that both the strength and dominant wave direction of microseismic noise can be estimated prior to an ocean-bottom experiment. Better estimates for required deployment periods for temporary ocean-bottom deployments can thus be derived from existing land data, and the station configuration might be optimized to suppress microseismic noise by means of frequency-wavenumber filtering.

A second finding is that microseismic noise at about 1 Hz, which is smaller than the noise at 0.25 Hz, is generated locally above the station by wind-driven waves. This has been postulated before (e.g., Babcock *et al.*, 1994; Webb, 1998) but is evidenced here with a new technique incorporating oceanic waveheights.

Detection Thresholds

Because of the long deployment times we were able to estimate the detection probabilities for *P* waves of teleseismic earthquakes. As a reference we choose events with different magnitudes at 70° epicentral distance and the two stations with the best fidelity. Below the microseismic noise band the detection thresholds for both deployments were similar: 75% probability to detect a M_W 6.0 event.

Large differences were found near the microseismic peak. Although there is almost no chance to detect even an M_W 7 event at 70° distance in the North Atlantic, such an event would be detected 50% of the time in the Tyrrhenian Sea. On the hydrophone, an M_W 7.5 event can be recorded 50% of the time in the Tyrrhenian Sea. The predicted very high detection threshold on the hydrophone channel in the microseismic band is in full agreement with our experience from inspecting waveforms. It demonstrates the importance of deploying full OBSs with four channels instead of only hydrophones in the North Atlantic or at other noisy places.

To summarize our experience with free-fall OBS, free-fall stations are usable for broadband seismological purposes although a more consistent quality could be achieved by a controlled launching system and improved station design. Burial of sensors would most likely further reduce the noise level in the low-noise notch, in particular, for the horizontal components but will not help in the microseismic frequency band where the largest noise levels occur. However, because noise-generation areas are far-distant, in many cases, small-scale arrays to attenuate microseismic noise would probably help.

Acknowledgments

The work was supported by the Deutsche Forschungsgemeinschaft (DFG), the Leitstelle für Mittelgrosse Forschungsschiffe, and the University of Hamburg. We thank the crews of the *FS Alexander-von-Humboldt* and the *Bjarni Saemundson* for their professional work under difficult sea conditions. Roger Sitko, Jörg Reinhardt, Martin Hensch, Andreas Wittwer, Jörg Petersen, and Viola Gaw helped with the cruises. Ernst Flüh, Jörg Bialas, and Rolf Herber provided invaluable advice on the technical aspects of the instrumentation; Rudi Widmer-Schniedrig provided the global WAM models and the DWD (Deutscher Wetterdienst) provided the WAMS in the North Atlantic. We thank the associate editor Jose Pujol, Spahr Webb, and one anonymous referee for their valuable comments and suggestions.

References

- Babcock, J., B. Kirkendall, and J. Orcutt (1994). Relationship between ocean bottom noise and the environment, *Bull. Seism. Soc. Am.* **84**, 1991–2007.
- Bromirski, P. D. (2001). Vibrations from the perfect storm, *Geochem. Geophys. Geosys.* **2**, doi 10.1029/2000GC000119.
- Collins, J., F. Vernon, J. Orcutt, R. Stephen, K. Peal, F. Woodings, F. Spiess, and J. Hildebrand (2001). Broadband seismology in the oceans: lessons from the Ocean Seismic Network Pilot Experiment, *J. Geophys. Res.* **28**, 49–52.
- Cox, Ch., Th. Deaton, and S. Webb (1984). A deep sea differential pressure gauge, *J. Atmos. Oceanic Technol.* **1**, 237–246.
- Crawford, W., and S. Webb (2000). Identifying and removing tilt noise from low-frequency (< 0.1 Hz) seafloor vertical seismic data, *Bull. Seism. Soc. Am.* **90**, 952–963.
- Dahm, T., M. Thorwart, E. Flueh, T. Braun, R. Herber, P. Favali, L. Beranzoli, G. D'Anna, F. Frugoni, and G. Smiriglio (2002). Ocean bottom seismological instruments deployed in the Tyrrhenian Sea, *Eos Trans.* **83**, 309, 314.
- Duennebie, F. K., and G. Sutton (1995). Fidelity of ocean bottom seismic observations, *Mar. Geophys. Res.* **17**, 535–555.
- Essen, H.-H., F. Krüger, T. Dahm, and I. Grevemeyer (2003). On the generation of secondary microseisms observed in northern and central Europe, *J. Geophys. Res.* **108**, 2506, doi 10.1029/2002JB0002338.
- Flueh, E., and J. Bialas (1999). Ocean bottom seismometers, *Sea Technol.* **40**, 41–46.
- Godin, O., and D. Chapman (1999). Shear-speed gradients and ocean seismo-acoustic noise resonances, *J. Acoust. Soc. Am.* **106**, 2367–2382.
- Hasselmann, K. (1963). A statistical analysis of the generation of microseisms, *Rev. Geophys.* **1**, 177–210.
- Hedlin, M., and J. Orcutt (1989). A comparative study of island, seafloor, and subseafloor ambient noise levels, *Bull. Seism. Soc. Am.* **79**, 172–179.
- Komen, G., L. Cavaleri, M. Donelan, K. Hasselmann, S. Hasselmann, and P. Janssen (1994). *Dynamics and Modelling of Ocean Waves*, Cambridge Univ. Press, New York, 1–532.
- Longuet-Higgins, M. (1950). A theory of the origin of microseisms, *Phil. Trans. R. Soc. London A* **243**, 2–36.
- McCreery, C. S., F. K. Duennebie, and G. H. Sutton (1992). Correlation of the deep ocean noise (0.4–30 Hz) with wind, and the Holu Spectrum—a worldwide constant, *J. Acoust. Soc. Am.* **93**, no. 54, 2639–2648.
- Peterson, J. (1993). Observation and modeling of seismic background noise, *U.S. Geol. Surv. Open File Rept.* 93-322, 1–49.
- Press, W., B. Flannery, S. Teukolsky, and W. Vetterling (1992). *Numerical Recipes*, Second Ed., Cambridge Univ. Press, New York.
- Ritsema, J., and R. M. Allen (2003). The elusive mantle plume, *Earth Planet. Sci. Lett.* **207**, nos. 1–4, 1–12.
- Stephen, R., F. Spiess, J. Collins, J. Hildebrand, J. Orcutt, K. Peal, F. Vernon, and F. Wooding (2003). Ocean seismic network of pilot ex-

- periment, *Geochem. Geophys. Geosys.* **4**, 1092, doi 10.1029/2002GC000485.
- Stutzmann, E., J.-P. Montagner, A. Sebai, W. Crawford, J.-L. Thiriot, P. Tarits, D. Stakes, B. Romanowicz, J.-F. Karczewski, J.-C. Koenig, J. Savary, D. Neuhauser, and S. Etchmedy (2001). Moise: a prototype multiparameter ocean-bottom station, *Bull. Seism. Soc. Am.* **91**, 885–891.
- Thorwart, M., and T. Dahm (2005). Wave field decomposition for passive ocean bottom seismological data, *Geophys. J. Int.* **163**, 611–621, doi 10.1111/j1365-246x.2005.02761.x.
- Webb, S. (1998). Broadband seismology and noise under the ocean, *Rev. Geophys.* **36**, 105–142.
- Webb, S., and W. Crawford (1999). Seafloor seismology and deformation under ocean waves, *Bull. Seism. Soc. Am.* **89**, 1535–1542.
- Webb, S., T. K. Deaton, and J. C. Lemire (2001). A Broadband ocean bottom seismometer system based on a 1 Hz natural period geophone, *Bull. Seism. Soc. Am.* **91**, 304–312.

Appendix A

To calculate cross-coupling transfer functions, we first selected several noise sequences that are free of larger events and recording artifacts such as spikes or clipped waveforms. We then cut each noise sequence into windows of 164 sec with 50% overlap between adjacent windows. Each window is mean removed and tapered with a Bartlett window to reduce spectral leakage (Press *et al.*, 1992). The transfer function between “source” component s and “response” component r , $T_{rs}(\omega)$, is then calculated in the frequency domain:

$$T_{rs}(\omega) = \frac{\langle A_s^*(\omega)A_r(\omega) \rangle}{\langle A_s^*(\omega)A_s(\omega) \rangle},$$

where $A_s(\omega)$ and $A_r(\omega)$ are the complex spectra of the source and response components, respectively, and $\langle \dots \rangle$ implies averaging over all windows of all sequences. (In the following equations the dependence on ω is assumed but not explicitly stated.) The amplitude of the transfer function thus obtained is set to zero at those frequencies where coherency drops below 0.7. The coherency is defined as

$$\gamma_{rs} = \frac{| \langle A_r^* A_s \rangle |}{\sqrt{\langle A_r^* A_r \rangle} \sqrt{\langle A_s^* A_s \rangle}}.$$

In a small transition region near the threshold the amplitudes are reduced. The predicted signal for component r is then $T_{rs}A_s$, which is subtracted from the observed signal A_r to obtain the corrected signal $A_{r'}$. Following Crawford and Webb (2000), we carry out the following steps to correct the vertical component z using the horizontal components x and y .

1. $A_{z'} = A_z - T_{zx}A_x$
 $A_{y'} = A_y - T_{yx}A_x$
2. $A_{z''} = A_{z'} - T_{z'y'}A_{y'}$

An equivalent technique can be applied to correct noise correlated between the vertical and pressure component, p .

$$3. A_{z'''} = A_{z''} - T_{z''p}A_p$$

where we assume that the pressure noise is not correlated with the horizontal components.

Figures A1 and 4 illustrate the application of the algorithm to ob28, the station where it was most effective. The coherence between horizontal and vertical components is high below ~ 0.12 Hz (Fig. A1b), and coherence between the pressure and vertical components is high in the microseismic band (0.15–0.3 Hz). The transfer function between the vertical and the y component exhibits a relatively flat amplitude response and a nearly constant phase below 0.12 Hz (Fig. A1c), which implies that the noise on the vertical component has the same shape as that of the horizontal components but smaller amplitudes (factor 0.11 for z/y and -0.05 for z/x , clearly visible in the time domain, too; see Fig. 4a,b). If interpreted purely as tilt and there is no difference between the gain for different channels, the amplitude of the transfer function is the tangent of the tilt angle, in this case implying a tilt angle of 7° . Tilts for the other stations are listed in Table 1. Another potential source of coherent noise could be oscillations of the frame. As mentioned previously, it is hard to determine the cause of the coherent signal without additional information. The transfer function above 0.12 Hz is unreliable because the coherency is low, and it is not used for further processing.

After subtracting the predicted, tilt-induced signal from the vertical, the noise PSD is reduced by a factor of 100–1000 in the coherent band (Fig. A1d) but remains above the noise level for the quietest instrument, which was ob21 during the deployment in the North Atlantic. The microseismic noise PSD is only marginally reduced by the pressure-based correction.

Note that the tilt correction in Figure A1 is applied at frequencies a little bit into the microseismic peak. In the microseismic peak, the application of the tilt correction would have no positive effect and would reduce signal as well as the noise.

Institut für Geophysik, Universität Hamburg
20146 Hamburg, Germany
(T.D.)

Bullard Laboratories, Department of Earth Sciences
University of Cambridge
Cambridge, United Kingdom CB3 0EZ
(F.T.)

IfM-GEOMAR
24148 Kiel, Germany
(J.P.M.)

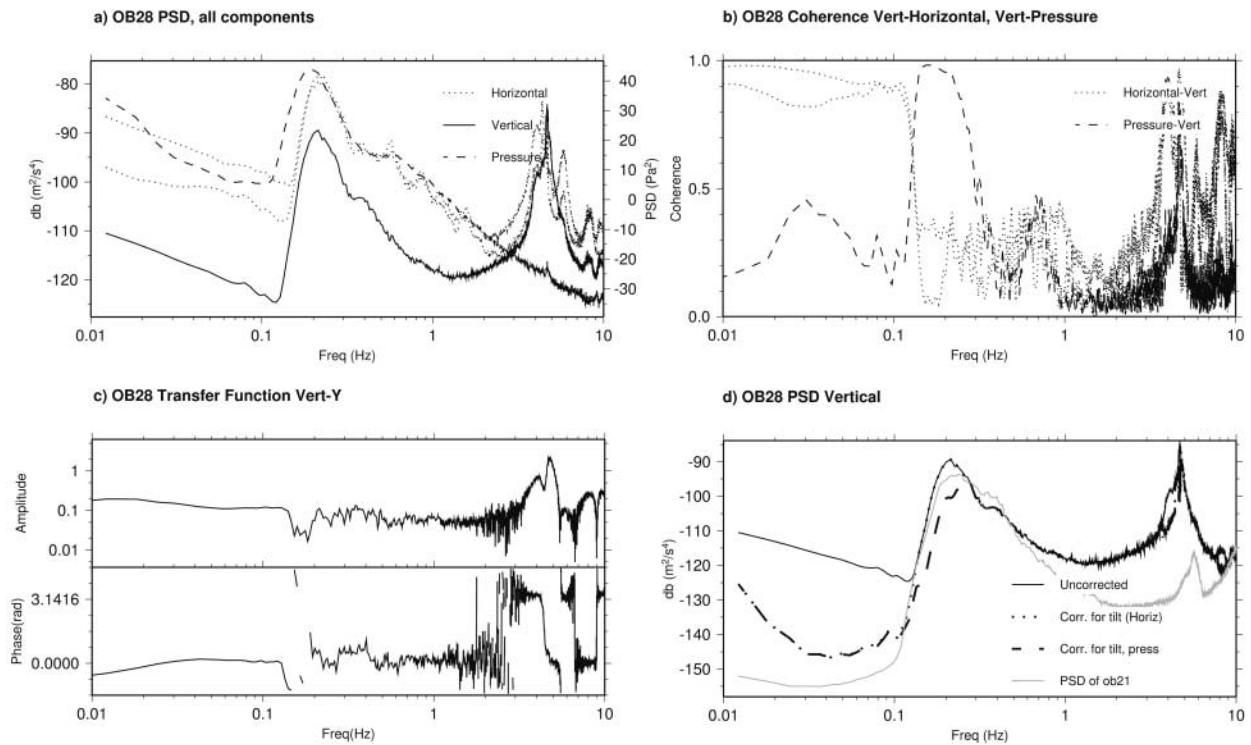


Figure A1. Tilt correction example for station OB28. (a) Noise PSD for all components. There are two horizontal curves for two horizontal channels; they have the same shape as the vertical but are noisier by 10–20 dB. (b) Coherency between the vertical noise and the pressure and two horizontal channels. (c) The empirically determined transfer function from the horizontal x component to the vertical component. Convolved with the noise on the x component, this function predicts the noise on the vertical channel. (d) Noise PSD for the vertical component. For the tilt-corrected signal (dashed line), the predicted noise from the horizontal components has been subtracted from the vertical components. For the tilt- and pressure-corrected signal (dotted line), the predicted noise from the pressure signal has been subtracted from the tilt-corrected signal. For comparison, the uncorrected noise PSD for ob21, the quietest station, has been superimposed (gray line). Below ~ 0.12 Hz, the dashed and dotted line lie on top of each other; above this frequency the dotted and continuous line lie on top of each other.